Catalysis Science & Technology

Accepted Manuscript

ROYAL SOCIETY OF CHEMISTRY

www.rsc.org/catalysis

Journal Name

ARTICLE

Recent Progress in g-C_3N_4 based low cost photocatalytic system: activity enhancement and emerging applications

Received 00th January 20xx,
Accepted 00th January 20xx

DOI: 10.1039/x0xx00000x

www.rsc.org/

Shengming Yin,[a] Jianyu Han,[ab] Tianhua Zhou,[ac] and Rong Xu[a*]

Graphitic C_3N_4 (g-C_3N_4) has continuously attracted attentions since it was reported as a metal free semiconductor for water splitting. However, its ability for evolving hydrogen from water is significantly dependent on the use of noble metal co-catalyst, mainly Pt. In recent years, a good progress has been achieved in developing co-catalysts containing earth abundant elements only for constructing low cost and efficient g-C_3N_4 based photocatalytic systems. Besides, exfoliation of bulk g-C_3N_4 into two dimensional g-C_3N_4 nanosheets offers large surface area and exposed active sites, which are beneficial for activity enhancement. Furthermore, oxygen evolution and CO_2 photoreduction over g-C_3N_4 have caught increasing interests due to the demand to achieve overall water splitting and conversion of CO_2 into chemicals and fuels. In this mini-review, we will briefly summarize the latest research works on g-C_3N_4 based photocatalytic systems during the last three years with emphasis on the progress achieved in enhancing hydrogen evolution activity of g-C_3N_4 by loading noble metal free co-catalysts, exfoliating bulk g-C_3N_4 into nanosheets, and the application of g-C_3N_4 system in photocatalytic O_2 evolution and CO_2 reduction.

1. Introduction

The energy and environment problems have become more and more severe over the recent years due to the overuse of fossil fuels and uncontrolled CO_2 emission from the combustion of fossil fuels. It is of utmost urgency to find green technology to address these concerns.[1] One promising method is the utilization of solar energy with the help of semiconductor photocatalysts. A process known as photocatalytic water splitting converts water into H_2 which is considered to be a promising clean energy to replace fossil fuels;[2] another process called artificial photosynthesis is focused on synthesizing hydrocarbon molecules from CO_2 which is a mimic of the natural photosynthesis in green plants.[3]

Since Fujishima reported a photoelectrochemical (PEC) water splitting process by TiO_2 photoanode, researchers have spent efforts on improving the conversion efficiency of this process.[4] Various semiconductors, e.g. oxide, (oxy)nitride, (oxy)sulfide have been shown capable of splitting water under light irradiation with suitable co-catalysts deposited on the surface.[5-7] Unfortunately, the relatively low efficiency and noble metal containing materials of these systems make them unfavourable for the practical usage. The price of H_2 by this method is still much higher than expected. Further improving the solar to hydrogen (STH) efficiency and reducing the cost are of particular significance to realize the potential of this technology. Compared to water splitting, the study of CO_2 photoreduction is still in its infancy partially due to the fact that it is energetically more difficult to reduce CO_2 than proton. CO_2 reduction requires a much larger driving force than water reduction (Table 1).[8] In addition, CO_2 reduction is a multiple electron process, which makes it kinetically harder to proceed. The selectivity of products is also an important aspect in CO_2 reduction. After all, the development of photocatalytic water splitting and CO_2 reduction depends on the efficient utilization of solar power and the enhancement of catalytic conversion of water and CO_2 into fuels and chemicals. These serve as the criteria for the selection of suitable photocatalysts.

Table. 1 CO_2 reduction potentials (reported at pH 7). Adapted with permission from ref. 8. Copyright 2009 American Chemical Society.

Reaction	$E^{0'}$ (V) vs SCE
$CO_2 + 2H^+ + 2e^- \rightarrow HCO_2H$	-0.85
$CO_2 + 2H^+ + 2e^- \rightarrow CO + H_2O$	-0.77
$CO_2 + 4H^+ + 4e^- \rightarrow C + 2H_2O$	-0.44
$CO_2 + 4H^+ + 4e^- \rightarrow HCHO + H_2O$	-0.72
$CO_2 + 6H^+ + 6e^- \rightarrow CH_3OH + H_2O$	-0.62
$CO_2 + 8H^+ + 8e^- \rightarrow CH_4 + 2H_2O$	-0.48

[a] School of Chemical & Biomedical Engineering, Nanyang Technological University, 62 Nanyang Drive, Singapore 637459. Fax: 65-67947553; Tel: 65-67906713; E-mail: rxu@ntu.edu.sg
[b] Energy Research Institute @ NTU, Nanyang Technological University, 50 Nanyang Drive, Singapore 637553
[c] SinBeRISE CREATE, National Research Foundation, CREATE Tower Level 11, 1 Create way, Singapore 138602

Graphitic carbon nitride (g-C_3N_4), also known as ñmelonò, is the most stable allotrope among different carbon nitride materials. It can be synthesized via thermal condensation of low cost nitrogen rich precursors such as cyanamide, dicyandiamide, melamine, thiourea and urea. It has a graphene-like structure consisting of two dimensional frameworks of tri-s-triazine connected via tertiary amines. This unique structure and high degree of condensation make g-C_3N_4 stable at elevated temperature as high as 600 ^oC and in different chemical environment (acid, base or organic solvent). Furthermore, this tri-s-triazine ring structure makes it an indirect semiconductor with a band gap of ~2.7 eV, corresponding to an optical wavelength of 460 nm in the visible light range.[9, 10] In 2009, Wang et al reported that photocatalytic water splitting can be achieved using this metal free polymeric g-C_3N_4.[11] Since then, enormous attention has been drawn on g-C_3N_4 because it is ideal for the construction of low cost photocatalysts. Nevertheless, the photoactivity of g-C_3N_4 suffers from several main drawbacks. Firstly, the relatively large band gap (2.7 eV) limits its effective utilization of visible light of longer wavelengths. It was estimated that a photocatalyst with a band gap as narrow as 1.8-2.0 eV and suitable band positions would be desirable from the viewpoint of both solar energy harvesting and surface kinetics of water splitting reactions.[12] Secondly, the low charge carrier mobility inhibits the separation and transportation of electrons and holes. It was revealed by both first principle calculations and experimental results that the charge carrier mobility of the pristine g-C_3N_4 can be enhanced by doping non-metal elements which widen the valence band (VB) of g-C_3N_4.[13-16] Furthermore, the surface inertness of g-C_3N_4 due to the nature of the covalent bonding leads to the low reaction rates of hydrogen and oxygen evolution half reactions.[9] The surface area of bulk g-C_3N_4 is generally small since it is prepared by condensation of organic precursor compounds under high temperature. There also exist rich grain boundary defects on the surface of g-C_3N_4 resulted from incomplete condensation, which may cause the recombination of excited charges.[17]

As a result, the efforts that have been made to address these issues include modification of the electronic structure of g-C_3N_4 by integrating certain organic molecules into its ring structure;[18, 19] doping metal or non-metal ions in the bulk structure of g-C_3N_4 to form impurity level in its forbidden band to improve its visible light absorption property;[14, 15, 20-23] and suppression of electron hole recombination by forming composites of g-C_3N_4 and other semiconductors with suitable band alignment or carbon materials to improve the charge transportation.[24-28] Sensitization of the pristine g-C_3N_4 by organic dyes or quantum dots is also efficient to enhance its performance under visible light.[29, 30] Besides, morphology control of g-C_3N_4 to increase the specific surface area as well as to expose active sites for photocatalytic reaction is another strategy to achieve photocatalytic activity improvement. Mesoporous g-C_3N_4 (mpg-C_3N_4) is commonly prepared using SiO_2 nanospheres as the template.[31] In addition, g-C_3N_4 with other morphologies such as spherical nanoparticle,[32] nanorod,[33-35] hollow sphere,[36, 37] and ordered 3D structure[38] have been prepared using template or non-template methods. There are many literature reports demonstrating the use of such modifications to improve the performance of g-C_3N_4 system, which has been shown as a promising material for solar fuel production.

In this mini review, we intend to summarize the recent progress on the development of efficient and low cost g-C_3N_4 systems on a few important aspects including deposition of noble metal free cocatalysts on g-C_3N_4, exfoliation of bulk g-C_3N_4 into g-C_3N_4 nanosheets and the application of g-C_3N_4 in water oxidation, overall water splitting and CO_2 photoreduction. These challenging research areas have drawn increasing interests from many research groups including our own. Some review articles have been recently published focusing on the fabrication, chemical modification, bandgap engineering and heterostructure formation of g-C_3N_4 based photocatalysts.[9, 10, 17, 28, 39] We believe this review would be a good complement to the literature on g-C_3N_4 based photocatalyst systems.

2. Noble metal free g-C_3N_4 system

Depositing suitable cocatalyst on the surface of semiconductor is of great importance to improve its efficiency. Cocatalysts significantly enhance the surface reaction rate by lowering the activation energy and facilitate the separation of electrons and holes by forming Schottky junction between semiconductor and cocatalyst. The role of cocatalyst on photocatalysis and photoelectrocatalysis has been well reviewed by Yang et al.[40]

Pt is so far the most efficient and commonly used cocatalyst of g-C_3N_4 for hydrogen production. Despite that a series of non-noble metal containing hydrogen evolution reaction (HER) electrocatalysts have been explored, only a few of them are successfully deposited on g-C_3N_4 as cocatalysts.[41] To further reduce the cost of the g-C_3N_4 based photocatalysts and make them available for industrial usage, noble metal free cocatalysts are highly needed.

As a pioneering work in this area, Dong et al reported in 2012 that a molecular cocatalyst $Ni(TEOA)_2Cl_2$ can be used in the system of g-C_3N_4 to replace Pt for stable hydrogen evolution.[42] In this system, g-C_3N_4 plays the main role of light absorber. $Ni(TEOA)_2Cl_2$ is formed via self-assembly of Ni^{2+} ions and triethanolamine (TEOA) which is the sacrificial reagent in solution. A similar nickel containing complex, nickel-thiourea-triethylamine (Ni-TU-TETN), formed *in situ* during photocatalytic reaction, was also reported to be an active cocatalyst on the surface of g-C_3N_4 for hydrogen production.[43] But the quantum efficiency (QE) obtained using Ni-TU-TETN/g-C_3N_4 is only 0.2% at 400 nm irradiation, which is much smaller than 1.51% at 400 nm reported for Ni-TEOA/g-C_3N_4. $Co(dmgH)_2pyCl$ has been studied as a electrocatalytic HER catalyst and was used for photocatalytic hydrogen production in a homogeneous system as well.[44] When coupled with g-C_3N_4 in TEOA solution, it was able to produce hydrogen under visible light. The highest QE of this system was 0.62% at 365 nm irradiation.[45] However, the activity decreased dramatically after 8 h of photocatalytic reaction due to the decomposition of $Co(dmgH)_2pyCl$. To overcome this, a more stable $Ni(dmgH)_2$ HER catalyst was used to construct a $Ni(dmgH)_2$/g-C_3N_4 photocatalyst. $Ni(dmgH)_2$ sub-microcrystals were grown on g-C_3N_4 via a simple precipitation method. Its activity remained almost the same after three recycle runs, indicating the enhanced stability of this system although the activity needs to be further improved.[46]

Besides the transition metal containing complexes, some inorganic compounds have also been coupled with g-C_3N_4 for the construction of noble metal free g-C_3N_4 photocatalysts. For example, our group has successfully deposited NiS on g-C_3N_4

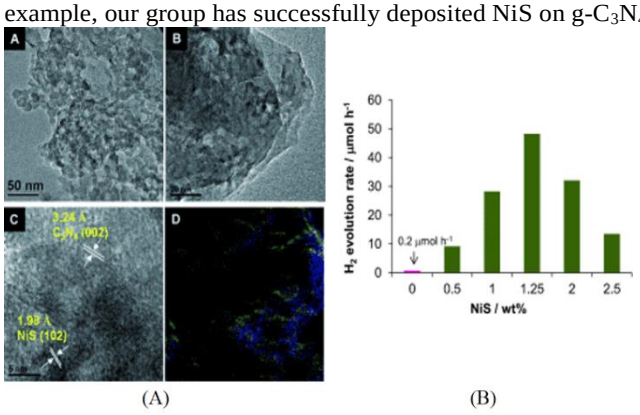

Fig. 1 (A) TEM, HRTEM and element mapping images of NiS/mpg-C_3N_4; (B) Effect of NiS cocatalyst loading on hydrogen production.[47] Copyright 2013 WILEY-VCH Verlag GmbH & Co. KGaA Weinheim.

via a facile hydrothermal method.[47] An aqueous solution of nickel acetate (NiAc) and thioacetamine was used for the synthesis of NiS in the presence of mpg-C_3N_4, allowing Ni^{2+} and sulfur precursor to enter into the pores of mpg-C_3N_4 for the formation of nanosized and well-dispersed NiS cocatalyst. The formation of NiS nanoparticles was confirmed by high resolution transmission electron microscopy (HRTEM) analysis, element mapping and X-ray photoelectron spectrum (XPS). The typical HRTEM images and elemental mapping results are shown in Fig. 1A. The loading of NiS has a significant effect on the activity and the optimum NiS loading was found to be 1.25 wt% (Fig. 1B). For comparison, the activity of a mixture of mpg-C_3N_4 and pre-synthesized NiS was much lower than that of NiS/mpg-C_3N_4, which is due to the poor interface between NiS and mpg-C_3N_4 and the relatively larger particle size of pre-synthesized NiS. A high QE of 1.9% at 440 nm was obtained over the optimized NiS/mpg-C_3N_4 photocatalyst. The same photocatalyst demonstrates a good stability with 84% of the initial activity retained after 4 runs of photoreaction. Subsequently, Chen et al reported the preparation of NiS/g-C_3N_4 via ion exchange that converts Ni^{2+}/g-C_3N_4 to NiS/g-C_3N_4 using Na_2S.[48] Another type of nickel sulfide supported on g-C_3N_4, NiS_2/g-C_3N_4, was prepared via a hydrothermal method using NiAc and thiourea in the presence of g-C_3N_4.[49] The activity of the optimized NiS_2/g-C_3N_4 system is 4 times that of Pt/g-C_3N_4. However, the activity dropped to 60% of the initial value after five cycles. All these results indicate that nickel sulfides represent promising cocatalysts for the construction of noble metal free g-C_3N_4 photocatalysts for hydrogen evolution. In addition, cobalt sulfide has been evaluated as the cocatalysts for mpg-C_3N_4[47, 50] and exhibited lower activities than NiS under the same conditions.[47]

In the family of metal sulfides, MoS_2 and WS_2 nanosheets have received a lot of interests as efficient noble free HER catalysts for both electrocatalytic and photocatalytic reactions.[51] MoS_2 or WS_2 have also been loaded on g-C_3N_4 to act as cocatalysts. It is expected that the nanosheet morphology of these catalysts can facilitate charge transfer between g-C_3N_4 and the catalyst. Furthermore, the thin layer structure of the nanosheets can minimize the light blocking effect by cocatalysts in the aggregated form. Both MoS_2/mpg-C_3N_4 and

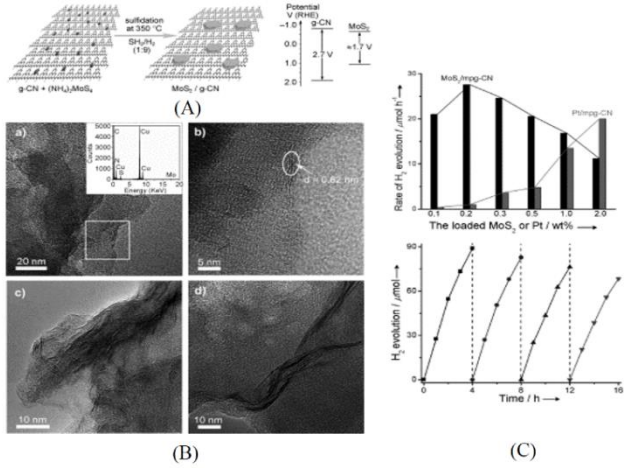

Fig. 2 (A) Schematic of MoS_2/mpg-C_3N_4 nanojunction and the band energy diagram; (B) TEM and HRTEM images of the MoS_2/mpg-C_3N_4; (C) hydrogen production rate of mpg-C_3N_4 loaded with MoS_2 or Pt and recycling behavior for 0.2wt% MoS_2/mpg-C_3N_4.[52] Copyright 2013 WILEY-VCH Verlag GmbH & Co. KGaA Weinheim.

WS_2/mpg-C_3N_4 were prepared by impregnation method.[52, 53] As schematically shown in Fig. 2A, $(NH_4)_2MoS_4$ or $(NH_4)_2WS_4$ was impregnated on mpg-C_3N_4 and the subsequent sulfidation was carried out in H_2S or H_2S/H_2 atmosphere at an elevated temperature. MoS_2 nanosheets were observed in HRTEM images (Fig. 2B). As can be seen in Fig. 2C, the activity of the optimized MoS_2/mpg-C_3N_4 was found higher than that of Pt/mpg-C_3N_4 and a QE of 2.1% was obtained at 400 nm. The stability of this system is also good with 80% of the initial activity maintained after recycling for four runs. Compared to MoS_2/mpg-C_3N_4, the activity of WS_2/mpg-C_3N_4 is relatively lower and decreased dramatically after recycled runs.

Hydroxides such as $Ni(OH)_2$ and $Cu(OH)_2$ were also reported to be capable of evolving hydrogen when coupled with g-C_3N_4.[54, 55] The preparation method of hydroxide/g-C_3N_4 was simply precipitating metal cations by NaOH with pre-added g-C_3N_4 followed by aging for a certain period of time. Both $Ni(OH)_2$/g-C_3N_4 and $Cu(OH)_2$/g-C_3N_4 were found to be stable and efficient for photocatalytic hydrogen production. A relatively high QE of 1.1% was obtained over $Ni(OH)_2$/g-C_3N_4 at 420 nm. XPS study for the hydroxide/g-C_3N_4 samples before and after photoreaction revealed that the *in situ* formed Ni^0 or Cu^0 cluster via reduction of metal ions by photo electrons is the key to the hydrogen production process.

Very recently, Zhang et al prepared a core shell structured Ni/NiO loaded on g-C_3N_4 by the impregnation method for hydrogen production.[56] Ni^{2+} on g-C_3N_4 was first reduced to Ni nanoparticles in H_2 flow and then the surface of Ni nanoparticles were oxidized to NiO after being annealed in air leading to the formation of core shell nanostructure. Ni/NiO-g-C_3N_4 showed improved activity for photocatalytic hydrogen production compared with the pristine g-C_3N_4, Ni-g-C_3N_4 and NiO-g-C_3N_4 due to the enhanced charge transfer across the interface. The overpotential for HER was also

reduced for Ni/NiO-g-C_3N_4, confirming that the Ni/NiO core/shell structure is a suitable catalyst for HER.

In short, various noble metal free g-C_3N_4 based photocatalysts have been investigated. It is promising to find that the activities of some photocatalysts approach or surpass those of Pt/g-C_3N_4. However, it is still challenging to prepare stable and efficient noble metal free g-C_3N_4 photocatalysts with their activities comparable or better than other semiconductor based systems. The photoelectric current and the photocatalytic efficiency are still low due to the drawbacks mentioned before. One of the possible solutions could be the development of new preparation methods to enhance the interface between the cocatalysts and g-C_3N_4. Furthermore, similar to the case of graphene, the electronic and morphological properties of g-C_3N_4 itself could be tuned by exfoliation to enhance the photocatalytic performances, which is discussed in the next section.

3. Generation of g-C_3N_4 nanosheets by exfoliation toward enhanced photocatalytic activity

Among various methods for control and modification of the morphology of g-C_3N_4, exfoliation is a simple and facile process which has been shown effective to enhance the photocatalytic performance of g-C_3N_4. Bulk g-C_3N_4 has a graphite like structure which contains elementary layers built up from ring structure of carbon nitride and van der Waals interaction between the layers. This unique structure makes g-C_3N_4 possible to be exfoliated into a graphene like single layered nanosheets. By exfoliating bulk g-C_3N_4 into nanosheets, the specific surface area can be increased and the catalytic centers are exposed. Furthermore, due to the quantum confinement effect, the conduction band (CB) position of g-C_3N_4 nanosheets can be shifted to more negative values than that of its bulk compartment, which provides a larger driving force for photocatalytic reaction.

The exfoliation methods of g-C_3N_4 can be classified as thermal exfoliation and liquid exfoliation. Niu et al reported the preparation of graphene like g-C_3N_4 nanosheets by thermal etching of bulk g-C_3N_4.[57] After the g-C_3N_4 sample was thermally oxidized in air at 500 ^oC for 2 h, g-C_3N_4 nanosheets with the thickness ranging from 1.62 nm to 2.62 nm were obtained corresponding to 4 to 7 carbon nitride layers. Compared to bulk g-C_3N_4, the optical absorption of g-C_3N_4 nanosheets exhibited 20 nm blue shift which is due to the quantum confinement. The surface area of g-C_3N_4 nanosheets increased from 50 m^2/g to 306 m^2/g. The synergistic effect of the higher surface area and the more negative CB position results in a significant increase in its hydrogen production activity. Xu et al further modified this thermal exfoliation method by firstly preparing a NH_4Cl/g-C_3N_4 composite with NH_4Cl intercalated in the interlayer space via hydrothermal reaction. Then the composite was annealed in N_2 to exfoliate g-C_3N_4 into nanosheets by the evolved gaseous NH_3.[58] The preparation method is schematically illustrated in Fig. 3A. The surface area of g-C_3N_4 nanosheets is 10 times that of the bulk g-C_3N_4 prepared using dicyanodiamide as the precursor. As shown in Fig. 3B, the average thickness of the as-prepared g-C_3N_4 nanosheets is around 2.8 nm measured by atomic force microscopy (AFM). Although thermal exfoliation is considered to be a low cost, large scale and environmentally friendly method for preparing g-C_3N_4 nanosheets, the highest yield of the nanosheets obtained so far is 6 wt% of the starting bulk g-C_3N_4.[57]

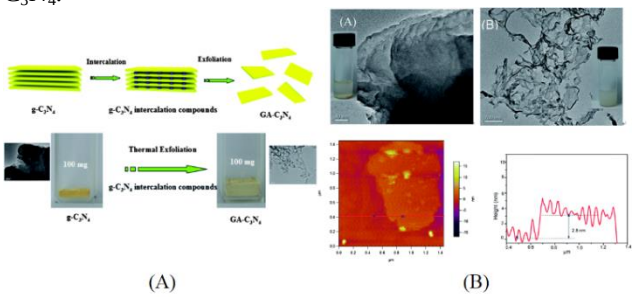

Fig. 3 (A) Schematics of thermal exfoliation of g-C_3N_4 into nanosheets and the optical images of g-C_3N_4 before and after exfoliation; (B) typical TEM images of bulk g-C_3N_4 and g-C_3N_4 nanosheets and AFM image and thickness profile of exfoliated nanosheets. Reproduced from ref. 58 with permission from The Royal Society of Chemistry.

Liquid exfoliation is a more commonly used method and is done by ultrasonication of bulk g-C_3N_4 material in a suitable solvent. After this process, the exfoliated nanosheets can be easily separated from the remaining bulk g-C_3N_4 by centrifugation. It is considered as a facile method for the preparation of 2D materials. Zhang et al firstly reported the preparation of g-C_3N_4 nanosheets using water as the solvent during ultrasonication.[59] As there is dangling hydrogen in the carbon nitride layer of g-C_3N_4, it was supposed that a polar solvent like H_2O is effective for the swelling and exfoliation of g-C_3N_4. The swelling and exfoliation process is shown in Fig. 4A. Besides H_2O, formamide, dimethylformamide, ethanol and methanol were used as exfoliation solvents. Only H_2O was found effective and the concentration of the resulting nanosheets suspension was measured to be 0.15 mg/mL. The change of UV-vis spectrum and photoluminescence (PL) spectrum before and after exfoliation can be attributed to the enlarged bandgap induced by quantum confinement (Fig. 4B). As shown in Fig. 4C, the thickness of as-prepared g-C_3N_4 naosheets is ~2.5 nm corresponding to 7 atomic layers and the lateral length of the nanosheets ranges from 70 nm to 140 nm. The as-prepared nanosheets were used for bioimaging due to its high PL quantum yield and biocompatibility. Inspired by this result, researchers have adopted the liquid exfoliation method for the preparation of g-C_3N_4 nanosheets and expanded the application of g-C_3N_4 nanosheets to other areas. For example, Sun and co-workers applied the same method and used the resulting nanosheets as an efficient fluoro-sensor for detection of Cu^{2+}.[60] Cheng et al exfoliated g-C_3N_4 in water and loaded Au nanoparticles on the exfoliated g-C_3N_4 nanosheets via photodeposition. The composite was found to be able to efficiently degrade methyl orange under visible light.[61] In addition, Zhang et al reported that the reaction pathway for photocatalytic phenol degradation is changed when exfoliated nanosheets were used as the photocatalyst.[62] In this case, g-C_3N_4 nanosheets with a thickness of 2 nm was prepared by

sonication in water. The change of bandgap and CB position were measured by UV-vis spectrum and Mott-Schottky plot. It was found that oxygen was reduced to H_2O_2 on g-C_3N_4 nanosheets via two electron transfer process while $\cdot O_2^-$ was formed on the surface of bulk g-C_3N_4 via one electron transfer process. This was attributed to the formation of 1,4-endoperoxide species on the surface of g-C_3N_4 nanosheets.

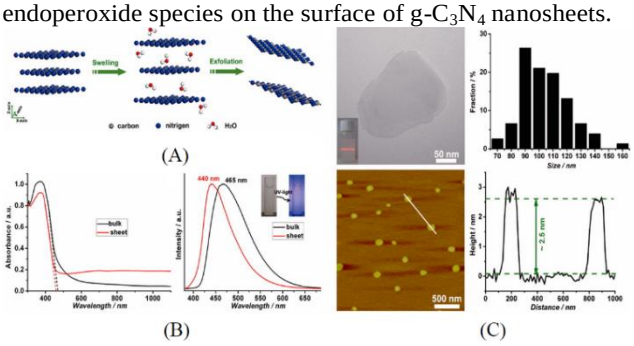

Fig. 4 (A) Schematics of the swelling and exfoliation of g-C_3N_4 by H_2O; (B) UV-vis spectrum and PL spectrum for bulk g-C_3N_4 and nanosheets; (C) typical TEM image and AFM image showing the lateral dimension and thickness of g-C_3N_4 nanosheets. Reprinted with permission from ref. 59. Copyright 2015 American Chemistry Society.

The two electron transfer pathway promoted the efficient separation of excited electrons and holes and facilitated the formation of reactive species which resulted in the enhanced photocatalytic activity for phenol degradation.

Besides water, other polar solvents or mixed solvent have also been investigated for the exfoliation of g-C_3N_4. For instance, isopropanol alcohol (IPA) was found another suitable solvent for exfoliation of g-C_3N_4 into nanosheets due to the surface energy matching of IPA and g-C_3N_4.[63] An extended sonication duration of 10 h yielded g-C_3N_4 nanosheets with an average thickness of 2 nm which is thinner than those prepared using H_2O as the solvent. Similarly, the exfoliated g-C_3N_4 nanosheets exhibited a high surface area of 384 m^2/g. The electrochemical impedance spectrum (EIS) results indicated an enhanced charge separation and transfer ability. Compared to bulk g-C_3N_4, the electron transfer resistance of g-C_3N_4 nanosheets decreased by 75%. The photocatalytic hydrogen production activity of g-C_3N_4 nanosheets is 10 times that of the bulk counterpart and is also higher than that of mpg-C_3N_4. In another work, She et al prepared g-C_3N_4 nanosheets via sonication in 1,3-butanediol (1,3-BUT).[64] Due to the polarity and surface energy matching, 1,3-BUT can swell and exfoliate g-C_3N_4 into nanosheets with a thickness of 0.9-2.1 nm. Mixed solvents have also been used for exfoliation of g-C_3N_4 such as the mixture of ethanol and water.[65] Interestingly, it was found that the ratio of the two solvents affect the yield and the highest concentration of nanosheets at 3 mg/mL was obtained with an ethanol/water volume ratio of 1:3. This concentration is much higher than that obtained in the single solvent. Furthermore, it is usual that g-C_3N_4 monolayer was obtained using such mixed solvents. Monolayer g-C_3N_4 nanosheets can also be produced via a combination of heat treatment and liquid exfoliation and the resultant nanosheets exhibited efficient photocatalytic disinfection activity for *Escherichia coli*.[66] Fig. 5 shows the EIS curves and transient photoresponse of the bulk and single-layered g-C_3N_4, indicating the enhanced charge transportation property of g-C_3N_4 nanosheets. Although facile and simple, the disadvantage of liquid exfoliation method is obvious. It usually takes long sonication duration and the yield is generally lower than 15%. In our recent work, the exfoliation of mpg-C_3N_4 in ethanol was carried out using a probe sonicator.[67] The probe sonicator with a higher power intensity is directly immersed

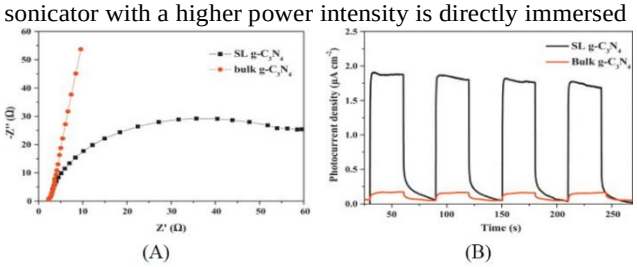

Fig. 5 (A) EIS of the bulk g-C_3N_4 and single-layered g-C_3N_4; (B) Transient photoresponse of bulk g-C_3N_4 and single-layered g-C_3N_4. Reprinted from ref. 65, Copyright 2015 with permission from Elsevier.

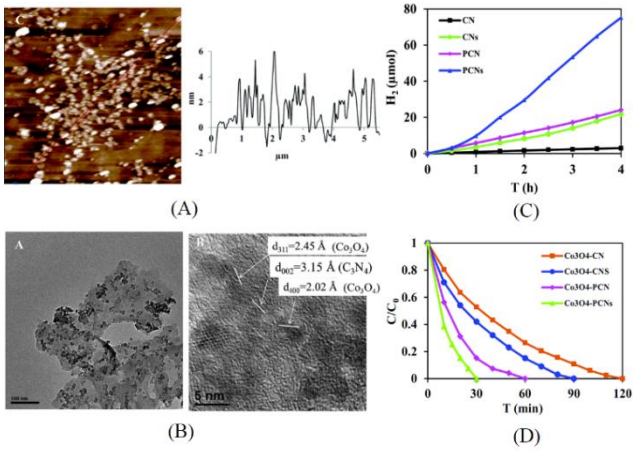

Fig. 6 (A) AFM image and the thickness profile of mpg-C_3N_4 nanosheets exfoliated using a probe sonicator; (B) TEM and HRTEM images of Co_3O_4/porous g-C_3N_4 nanosheets; (C) hydrogen production over Pt loaded g-C_3N_4 samples under visible light; (D) degradation of Rhodamine B over Co_3O_4 loaded g-C_3N_4 samples under UV-vis light (CN: g-C_3N_4, CNs: exfoliated g-C_3N_4 nanosheets, PCN: mesoporous g-C_3N_4, PCNs: exfoliated mesoporous g-C_3N_4 nanosheets). Reproduced from ref. 67 with permission from The Royal Society of Chemistry.

into the suspension and hence is much more effective than a bath sonicator. It is widely used in the exfoliation of layered metal chalcogenide like MoS_2.[68] The resultant yield (25.8%) for exfoliated mpg-C_3N_4 nanosheets was much higher than the previous reported values. Shown in Fig. 6A, the thickness of such mpg-C_3N_4 nanosheets was 2-3 nm in average, corresponding to 5-8 carbon nitride layers. After depositing Pt or Co_3O_4 on the surface of mpg-C_3N_4 nanosheets as cocatalysts (Fig. 6B), the photocatalytic activities for hydrogen evolution or degradation of Rhodamine B, respectively, were greatly enhanced compared to those of the bulk g-C_3N_4 (Fig. 6C and D). It is remarkable that the hydrogen evolution rate is 26 times that of the bulk g-C_3N_4.

Inspired by the Hummers method for the exfoliation of graphite into graphene, Zhu et al developed a chemical etching method for the preparation of single atomic layered g-C_3N_4 nanosheets.[69] It was found that only nanoparticles were obtained in the presence of $KMnO_4$ since g-C_3N_4 is not stable enough against the oxidation by $KMnO_4$.[57] H_2SO_4 (98%) was firstly intercalated into the interlayer

space of g-C_3N_4. Then g-C_3N_4 nanosheets were obtained by the rapid heating effect of H_2SO_4 (98%) mixed with water. The yield of g-C_3N_4 nanosheets reached as high as 30%. AFM observation revealed that the thickness of 60% of the exfoliated nanosheets was around 0.4 nm which is close to the theoretical thickness of a single carbon nitride layer. Correspondingly, the surface area was significantly increased from 4.3 m^2/g to 205.8 m^2/g after exfoliation. After loading Pt on the surface of as-prepared g-C_3N_4 nanosheets, it exhibited an enhancement factor of 2.6 for hydrogen evolution compared to bulk g-C_3N_4. A subsequent research work demonstrated that the surface charge of the nanosheets prepared using this chemical etching method can be tuned by adding different charge guest. The electrostatic assembly of g-C_3N_4 nanosheets with CdS or BiOBr was prepared and investigated for the photocatalytic degradation of methyl orange (MO) and aminobenzoic acid.[70] The CdS/g-C_3N_4 nanosheets composite exhibited a superior photocatalytic activity. However, before the nanosheets can be used for photocatalytic reaction, the suspension should be carefully and thoroughly washed to fully remove the acid.

Besides the abovementioned research efforts, the exfoliated g-C_3N_4 nanosheets have also been coupled with other materials such as carbon nanotube, reduced graphene oxide and WO_3 arrays via electrostatic interaction for potential application in electrocatalysis or PEC reactions.[71-74] In summary, g-C_3N_4 can be effectively exfoliated into monolayer or few layered nanosheets in polar solvents including water, some organic solvents and acid solution or by a simple thermal exfoliation. The exfoliated nanosheets present enhanced photocatalytic or PEC activities due to larger specific surface area, enhanced charge separation and transfer ability and more negative CB. The exfoliation process is simple but time consuming and the yield of nanosheets is generally low. Another main disadvantage for sonication assisted exfoliation method is that boundary defects may be induced during the treatment which may lead to the charge recombination. So far, we are unable to synthesize larger domain sizes with current synthetic scheme.[12] Further development of efficient and economic preparation methods for g-C_3N_4 nanosheets is needed for their practical applications.

4. g-C_3N_4 based photocatalysts for oxygen evolution and overall water splitting

Water oxidation, the other half reaction in overall water splitting, is a four electron transfer process and considered to be the rate limiting step in overall water splitting. Most of the research efforts on g-C_3N_4 based photocatalysts have been focused on the water reduction half reaction, which is proceeded in the presence of a hole scavenger. There are only limited studies on water oxidation by g-C_3N_4 system, not to mention overall water splitting. Despite the energetic barrier and sluggish kinetics, water oxidation by g-C_3N_4 also suffers from the self-oxidation of the catalyst which leads to the evolution of N_2 similar to the case of (oxy)nitrides e.g. Ta_3N_5, $LaTiO_2N$.[75] Efficient cocatalyst and protection layer need to be developed to mitigate this problem.

When g-C_3N_4 was first reported to be active for water splitting, its oxygen evolution activity was studied using $AgNO_3$ as the electron acceptor.[11] With RuO_2 loaded as a water oxidation catalyst (WOC), g-C_3N_4 was shown to be able to oxidize water into O_2 with a low reaction rate. Maeda et al showed that the photocorrosion can be significantly inhibited by loading RuO_2 as an efficient WOC. Otherwise the evolution of N_2 is significant.[76] When the loading amount of RuO_2 was optimized to 3 wt%, the highest oxygen evolution rate was obtained (12 μmol/h). McMillan et al studied the effect of the precursor and reaction parameter during g-C_3N_4 preparation on its oxygen evolution activity with RuO_2 as the cocatalyst.[77]

Besides the aforementioned drawbacks of g-C_3N_4, one of the main factors limiting its water oxidation activity is its VB edge position at about 1.4 V *vs.* NHE.[11, 14, 15] Compared to the VB position of widely studied oxides such as WO_3 (2.7 V *vs.* NHE), $BiVO_4$ (2.8 V *vs.* NHE) and Fe_2O_3 (2.2 V *vs.* NHE), g-C_3N_4 can only provide moderate water oxidation ability.[78] Wang and co-workers used trithiocyanuric acid as the precursor to prepare sulfer-mediated g-C_3N_4 (CNS).[79] After condensation, the sulfur amount in the final product was less than 1 wt%. The release of sulfur species during synthesis altered the connectivity pattern, topology of g-C_3N_4 and lowered the VB position by *ca.* 0.2 V. It showed a 4-fold increase in O_2 production compared to the pristine g-C_3N_4. However, the oxygen production rate of CNS was only 2.5 μmol/h under visible light irradiation since the photocatalytic experiment was conducted without loading a suitable WOC.

Then, the same group loaded cobalt species as WOC on CNS by an impregnation method and constructed an efficient noble-metal free photocatalysis system for water oxidation.[80] The structure of the cocatalyst was confirmed to be mainly Co_3O_4 by XPS and HRTEM. Fluorescence quenching study indicated efficient charge transfer from CNS to Co_3O_4. The PEC study showed that Co_3O_4/CNS lowered the onset potential of anodic photocurrent by 120 mV and also enhanced the photocurrent response. Using $AgNO_3$ as electron acceptor, the optimized Co_3O_4/CNS exhibited an oxygen evolution rate of 25.1 μmol/h under visible light. However, the oxygen evolution rate gradually decreased after 5 h which could be due to the deposition of Ag nanoparticles which blocked the catalytic centers as well as light absorption. Recently, Zhang et al reported the deposition of another cobalt based cocatalyst, $Co(OH)_2$, on the surface of g-C_3N_4 via simple precipitation (Fig. 7A). The PL quenching study in Fig. 7B revealed the efficient charge transfer from g-C_3N_4 to $Co(OH)_2$. During the first hour,

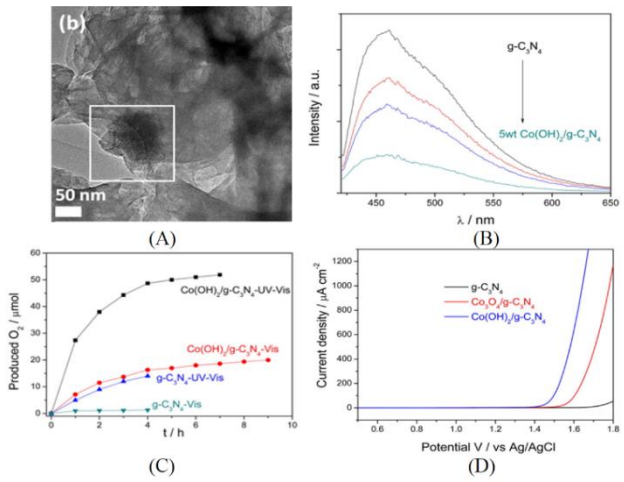

Fig. 7 (A) TEM image of $Co(OH)_2/g\text{-}C_3N_4$; (B) PL quenching of $g\text{-}C_3N_4$ and $Co(OH)_2/g\text{-}C_3N_4$; (C) photocatalytic oxygen production over $g\text{-}C_3N_4$ and $Co(OH)_2/g\text{-}C_3N_4$ under different conditions; (D) linear sweep voltammetry of different samples. Reprinted with permission from ref. 81. Copyright 2015 American Chemistry Society.

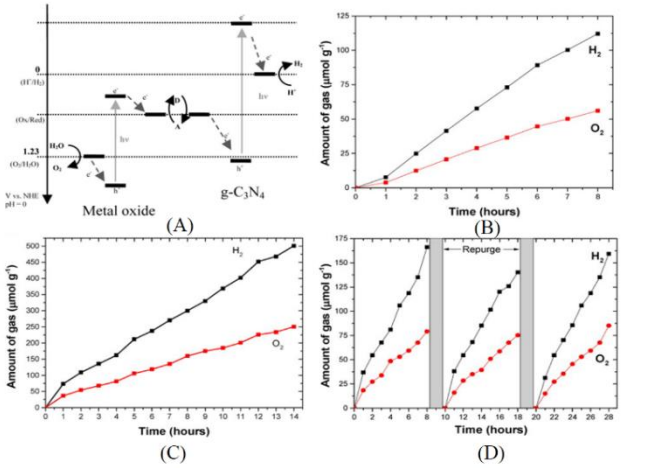

Fig. 8 (A) Schematics of Z-scheme photocatalysts constructed using $g\text{-}C_3N_4$ as the H_2-evolving photocatalyst and metal oxides as the O_2-evolving photocatalyst; overall water splitting over (B) $g\text{-}C_3N_4\text{-}FeCl_2\text{-}BiVO_4$ under full arc irradiation; (C) $g\text{-}C_3N_4\text{-}NaI\text{-}WO_3$ under full arc irradiation; (D) $g\text{-}C_3N_4\text{-}NaI\text{-}WO_3$ under visible light irradiation. Reprinted with permission from ref. 84. Copyright 2015 American Chemistry Society.

the oxygen evolution rate obtained was 27.4 μmol/h under UV-vis light irradiation (Fig. 7C).[81] After calcination in air, $Co(OH)_2/g\text{-}C_3N_4$ can be converted to $Co_3O_4/g\text{-}C_3N_4$, which is less active. Furthermore, the electrocatalytic oxygen evolution reaction (OER) onset potential of $Co(OH)_2/g\text{-}C_3N_4$ was found lower than that of $Co_3O_4/g\text{-}C_3N_4$ by the linear sweep voltammetry shown in Fig. 7D.

In the area of overall water splitting by $g\text{-}C_3N_4$ based system, only limited literature has been found reporting the successful construction of $g\text{-}C_3N_4$ photocatalysts that can evolve H_2 and O_2 simultaneously at a stoichiometric ratio. Lee et al decorated cobalt phosphate (CoPi) catalyst on the surface of $mpg\text{-}C_3N_4$ via direct photodeposition of Co^{2+} ions in a phosphate buffer solution or first deposition of metallic cobalt nanoparticles and then conversion of metallic nanoparticles to CoPi on $mpg\text{-}C_3N_4$.[82] The as-prepared $CoPi/mpg\text{-}C_3N_4$ is active for both HER and OER half reactions in the presence of suitable hole and electron scavenger, respectively. CoPi, a widely studied OER catalyst, was found to be converted *in situ* to Co-oxo/hydroxo-phosphate which is an active electrocatalyst for HER when a hole scavenger exists. In the absence of any charge scavenger, $CoPi/mpg\text{-}C_3N_4$ was found to be able to split water into H_2 and O_2 at the stoichiometric ratio in phosphate buffer solution with H_2 and O_2 produced at 13.6 μmolg/h and 6.6 μmol/g/h, respectively. The activity for overall water splitting is stable after three runs. Though the reaction rate is still very low, this is the first example of overall water splitting by $g\text{-}C_3N_4$ based photocatalyst.

Besides the single particulate system described earlier, Z-scheme photocatalyst which contains two photon systems is another way to achieve overall water splitting. Inspired by natural photosynthesis, Z-scheme system is composed of a H_2-evolving photocatalyst, an O_2-evolving photocatalyst and an electron mediator. Photocatalysts that are only active for half reactions can be employed to construct Z-scheme system, which extends the choice of the photocatalysts for overall water splitting. However, the activity of a Z-scheme system depends highly on a suitable combination of its components. So far the most active Z-scheme system employs $Ru/SrTiO_3$:Rh and $BiVO_4$ as H_2-evolving photocatalyst and O_2-evolving photocatalyst, respectively.[83] Other photocatalysts such as metal oxynitrides or metal sulfides are less active or inactive for Z-scheme system. Tang and his co-workers for the first time constructed a Z-scheme system employing $g\text{-}C_3N_4$ as H_2-evolving photocatalyst.[84] The mechanism is illustrated in Fig. 8A. Both $BiVO_4$ and WO_3 were used as the O_2-evolving photocatalyst and soluble Fe^{3+}/Fe^{2+} and IO_3^-/I^- pairs were used as electron mediator. With a such scheme, stoichiometric H_2 and O_2 were produced. As shown in Fig. 8, $g\text{-}C_3N_4\text{-}NaI\text{-}WO_3$ was the most efficient in this Z-scheme configuration with production rates of H_2 and O_2 at 74 μmol/g/h and 37 μmol/g/h, respectively, under full arc irradiation. The stability of this system is also confirmed to be good as stoichiometric H_2 and O_2 are evolved after three recycling runs and the gas production rate is almost the same as the initial run (Fig. 8D). Very recently, an effort was taken on the construction of mediator free Z-scheme overall water splitting system using $g\text{-}C_3N_4$ and WO_3 as the HER and OER photocatalysts, respectively.[85] The $g\text{-}C_3N_4\text{-}WO_3$ composite was synthesized by *in situ* growth of WO_3 on the surface of $g\text{-}C_3N_4$ in a hydrothermal reaction. In addition, they used reduced graphene oxide (rGO) as electron mediator which is expected to enhance the performance. After loading Pt as the cocatalyst, the photoactivity of $g\text{-}C_3N_4\text{-}WO_3$ and $g\text{-}C_3N_4/rGO\text{-}WO_3$ were measured in pure water without redox couples such as I^-/IO_3^-. Stoichiometric H_2 and O_2 can be stably evolved under visible light irradiation. A QE of 0.9% was obtained with the optimized sample at 420 nm. These results indicate that the intimate contact between two photocatalysts and improved electron transfer ability may benefit the H_2/O_2 evolution in the two step photoexcitation Z-scheme system. Further improvement of the activity of these systems is still needed.

Recently, Kang et al constructed a metal free $g\text{-}C_3N_4$ based composite photocatalyst by coupling $g\text{-}C_3N_4$ with carbon dots (CDs).[86] The Solar to hydrogen (STH) efficiency reached 2% for the optimized $CDs/g\text{-}C_3N_4$ system, which is much higher than the thus reported values for photocatalytic systems except that of CoO (5.1%) which is self-corroded within 1 h.[87] Such a STH efficiency reaches not far from the value of 5% set by the U.S. Department of Energy,

which corresponds to the H_2 production cost of $2.3/kg. Furthermore CDs/g-C_3N_4 exhibited long term stability for 200 days with the catalyst being separated, dried and reused after each day. The high stability can be attributed to its chemical and structure stability. A two-step OER mechanism including H_2O_2 production and subsequent decomposition of H_2O_2 to O_2 was found to be key to the high STH efficiency. This two-step pathway was verified by electrochemical study and shown to be faster than conventional four-electron process. Thus the STH efficiency was increased by accelerating the rate-limiting step of OER.

In summary, non-noble metal containing g-C_3N_4 based system is capable of efficiently evolving O_2 and is promising in overall water splitting. The metal free feature of g-C_3N_4 makes it a promising platform for the construction of low cost photocatalytic system to further lower the cost of solar fuel production.

5. CO_2 reduction using g-C_3N_4 based photocatalysts

CO_2 reduction is a rapidly developing research area as this technology provides possible solutions to the environmental and energy problems we are facing. Many studies and reviews have been published showing the promising findings in reduction of CO_2 into value added products.[1, 3, 8, 88-91] Similar to the situation in water oxidation and overall water splitting, there have not been extensive studies on CO_2 photoreduction by g-C_3N_4 based system. Nevertheless, during the last few years, CO_2 photoreduction using g-C_3N_4 has received increasing attention due to the interesting properties of g-C_3N_4 that may offer some opportunities in this area.

In 2012, Dong and co-workers prepared g-C_3N_4 and porous g-C_3N_4 by heating melamine or melamine hydrochloride and investigated their photocatalytic CO_2 reduction activity in the presence of water vapor under visible light.[92] Under these reaction conditions, CO was obtained as the reduction product. Subsequently, Mao et al reported the use of g-C_3N_4 with different microstructures for CO_2 photoreduction in NaOH solution without depositing any cocatalysts.[93] In this work, urea and melamine were used for the preparation of g-C_3N_4. It was found that the specific surface area of u-g-C_3N_4 (39.5 m^2/g) is much higher than that of m-g-C_3N_4 (3.7 m^2/g), which leads to more efficient surface adsorption, better charge separation and improved photoactivity. The CO_2 reduction products over u-g-C_3N_4 were CH_3OH and C_2H_5OH while only C_2H_5OH was produced over m-g-C_3N_4. It is interesting that hydrocarbons were produced by CO_2 reduction over g-C_3N_4 system instead of gaseous CO possibly because the reaction was conducted in aqueous solution. However, CH_3OH or C_2H_5OH may be oxidized on the surface of g-C_3N_4 by *in situ* evolved O_2 during long photoreaction indicated by the decreased reaction rate after irradiation beyond 9 h. Tuning the electronic structure of g-C_3N_4 by doping S into the pristine g-C_3N_4 can enhance its optical adsorption as well as the CO_2 reduction activity. S doped g-C_3N_4 was prepared by the condensation of thiourea and the CH_3OH yield over S doped g-C_3N_4 is 1.4 times that over the pristine g-C_3N_4.[94] To construct more efficient systems, one strategy is to couple the highly active homogeneous catalyst with g-C_3N_4. For instance, a Ru complex, cis,trans-[Ru{4,4ô-($CH_2PO_3H_2$)2-2,2ô-bipyridine}$(CO)_2Cl_2$]) (**Ru**) was adsorbed on the surface of mpg-C_3N_4 with a high surface area of 180 m^2/g.[95] The **Ru**/mpg-C_3N_4 was able to reduce CO_2 into formic acid under visible light while a small amount of H_2 and CO were also detected in acetonitrile in the presence of TEOA as the sacrificial reagent. Isotopic measurement result indicated that formic acid entirely came from CO_2 reduction while 77% of the evolved CO originated from the carbonyl ligand unit of **Ru** catalyst. The detachment of carbonyl ligand from **Ru** was a slow process and has also been reported in other papers including homogeneous and heterogeneous systems.[96, 97] However, the photocatalytic activity of **Ru**/mpg-C_3N_4 for formic acid production was found to stay almost unchanged even after 5 h of reaction. The **Ru** catalyst after carbonyl ligand detachment was expected to be the active species for CO_2 reduction. Subsequently, the same group studied the effect of pore-wall structure of mpg-C_3N_4 and the effect of **Ru** complex structure on CO_2 photo reduction.[98, 99] Based on these results, it is understood that the photoactivity is sensitive to the specific surface area of mpg-C_3N_4 and is not related to the pore size and volume. Furthermore, introduction of too much meso-porosity results in the shrinkage of mpg-C_3N_4 walls and leads to activity drop. With ï PO_3H_2 used as the linker group, **RuP**/mpg-C_3N_4 efficiently reduce CO_2 to HCOOH under visible light in N,N-dimethylacetamide with TEOA as the sacrificial reagent. This hybrid material gave a high turnover number (TON) of larger than 1000 and QE of 5.7% at 400 nm. In another study, Lin et al prepared $Co(bpy)_3Cl_2$/g-C_3N_4 hybrid material by self-assembly as the photocatalyst for reduction of CO_2 in acetonitrile under visible light in the presence of TEOA.[100] CO and H_2 were the main products. A TON of 4.3 with a relatively high selectivity of 88.4% for CO production were obtained by the optimized hybrid system. The surface of g-C_3N_4 or mpg-C_3N_4 was also modified with cobalt species as oxidative promoters to enhance CO_2 photoreduction. $Co(bpy)_3Cl_2/CoO_x$/mpg-C_3N_4 resulted in the highest TON of 13 and the selectivity of CO to H_2 is 78.5%. Noble metal cocatalysts loaded g-C_3N_4 have also been used for CO_2 photoreduction. Under UV-vis light CO_2 can be reduced to hydrocarbons (mainly CH_4, CH_3OH and HCHO) using Pt/g-C_3N_4 photocatalyst.[101] Pt acts as an electron sink to enrich the surface of g-C_3N_4 with electrons for efficient CO_2 reduction. The maximum yield can be obtained when the loading amount of Pt was 0.75%. However, Pt can also act as a catalyst for oxidation of HCHO over the time. Pt/g-C_3N_4 was also prepared via a polyol process and used for photoreduction of CO_2 in the presence of water vapor under day light lamp irradiation.[102] CH_4 was the main product from CO_2 reduction and 5.1 fold enhancement of CH_4 production was obtained after 2% Pt was loaded on g-C_3N_4.

The composites of g-C_3N_4 and metal oxides have been investigated by various research groups for CO_2 photoreduction. As in the case of hydrogen production, coupling g-C_3N_4 with a suitable semiconductor enhances the charge separation via band alignment, which leads to increased activity. For example, the composite of $NaNbO_3$ nanowires and g-C_3N_4 was prepared by annealing the mixture of $NaNbO_3$ nanowires and melamine at 520 ^oC in air.[103] In this case, g-C_3N_4 was expected to grow on the surface of $NaNbO_3$ and thus to make a good interface, which is revealed by the SEM and TEM images in Fig. 9B and C. The band energy diagram of $NaNbO_3$ and g-C_3N_4 is shown in the schematics in Fig. 9A. The suitable band alignment

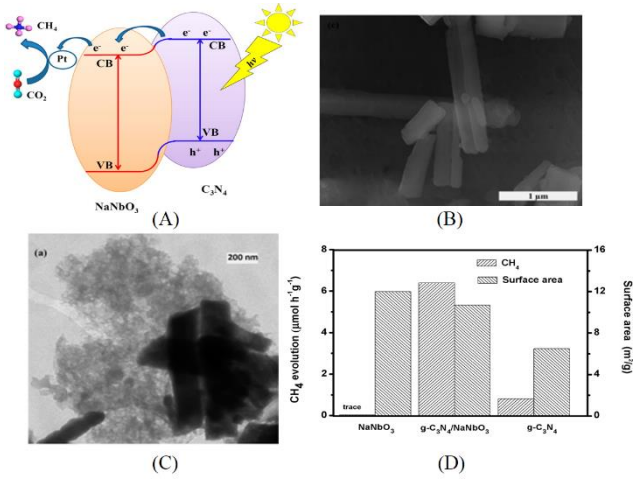

Fig. 9 (A) Schematics of energy diagram of $NaNbO_3$/g-C_3N_4; (B) SEM image and (C) TEM image of $NaNbO_3$/g-C_3N_4; (D) photocatalytic CO_2 reduction and surface area of $NaNbO_3$/g-C_3N_4. Reprinted with permission from ref. 103. Copyright 2015 American Chemistry Society.

between $NaNbO_3$ and g-C_3N_4 facilitates the charge separation in the composite. After photodeposition of 0.5% Pt, the composite was capable to reduce CO_2 to CH_4 and the activity was much higher than those of the individual components loaded with Pt. Cao et al prepared In_2O_3/g-C_3N_4 photocatalyst by a solvothermal method in dimethyl sulfoxide.[104] In_2O_3 nanocrystals were grown on the surface of sheet-like g-C_3N_4. In_2O_3/g-C_3N_4 exhibited a similar optical adsorption property as the pristine g-C_3N_4 but the transient photoresponse showed an increased photocurrent for In_2O_3/g-C_3N_4. After loading Pt as electron sink over 10% In_2O_3/g-C_3N_4, 159.2 ppm CH_4 can be evolved during 4 h. Transient PL decay indicated the inhibited charge recombination in In_2O_3/g-C_3N_4 due to enhanced charge separation at the interface. In another study, g-C_3N_4/TiO_2 heterojunction was prepared by an *in situ* growth method.[105] The surface area of the composite increased with the percentage of TiO_2 in the composite. When the photoreduction of CO_2 was carried out with water vapor without cocatalyst under UV-vis irradiation, CO was found as the main product although a small amount of CH_4 was also produced. Bi_2WO_6 was previously prepared by a hydrothermal method and shown active for the reduction of CO_2 into CO under visible light.[106] A solvothermal process was used to grow Bi_2WO_6 *in situ* to form g-C_3N_4/Bi_2WO_6 composite.[107] The measured CB and VB positions of g-C_3N_4 and Bi_2WO_6 were used to explain the possible mechanism for the photoreduction of CO_2 to CO. Compared to the pure Bi_2WO_6 prepared using the hydrothermal or solvothermal method, the activity of the composite was largely enhanced. ZnO, a large band gap semiconductor, was also used to make a composite with g-C_3N_4 by the impregnation method for the CO_2 reduction. The charge separation and transportation were promoted by the suitable band alignment between g-C_3N_4 and ZnO, which leads to an enhanced activity.[108] Besides oxides, carbon materials have also been coupled with g-C_3N_4 for CO_2 photoreduction. For example, a sandwich-like graphene/g-C_3N_4 hybrid nanostructure was fabricated using graphene oxide as a structure directing agent.[109] The hybrid material shows enhanced activity for the conversion of CO_2 to CH_4 in the presence of water vapor under a daylight lamp. The enhanced photoactivity was attributed to the improved electron transfer induced by graphene.

Besides the electronic and catalytic aspects, modifying g-C_3N_4 with a component for CO_2 adsorption and enrichment has been found effective in enhancing the performance of the overall system. For example, Wang et al coupled g-C_3N_4 with a Co-containing zeolitic imidazole framework (Co-ZIF).[110] Co-ZIF-9 has a high CO_2 adsorption capacity of 2.7 mmol/g and affords a high microporous surface area of 1607 m^2/g. As a result, Co-ZIF-9 can capture and concentrate CO_2 in its pores. After an electron mediator, bipyridine, was added into the reaction solution, the photoexcited electrons can be transferred from g-C_3N_4 to Co-ZIF-9 for CO_2 reduction as revealed by PL quenching study. CO was the main product in this system and a QE of 0.9% can be obtained, even without the loading of a cocatalyst. Our group reported the construction of a hybrid system using g-C_3N_4 and an anionic clay called layered double hydroxide (LDH) which has

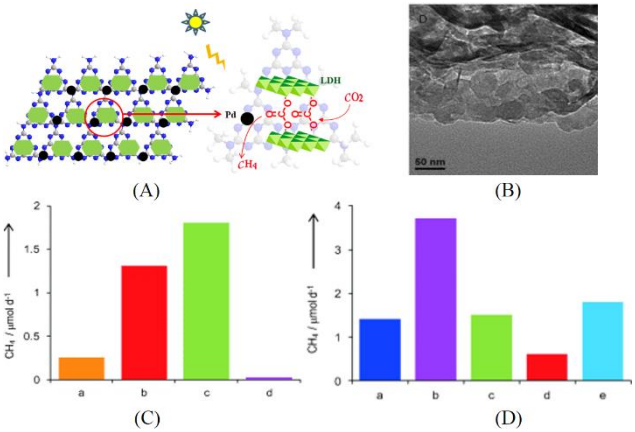

Fig. 10 (A) Schematics of the structure of Mg-Al-LDH/g-C_3N_4; (B) TEM image of Mg-Al-LDH/g-C_3N_4; (C) CO_2 reduction activity of Pd loaded photocatalysts, a. LDH-NO_3^-/g-C_3N_4, b. LDH/g-C_3N_4, c. LDH-CO_3^{2-}/g-C_3N_4, d. g-C_3N_4; (D) CO_2 reduction activity of Pd loaded photocatalysts, a. g-C_3N_4, b. Mg-Al-LDH/g-C_3N_4, c. Zn-Al-LDH/g-C_3N_4, d. Ni-Al-LDH/g-C_3N_4, e. Zn-Cr-LDH/g-C_3N_4.[111] Copyright 2014 WILEY-VCH Verlag GmbH & Co. KGaA Weinheim.

high affinity for CO_2.[111] The structure of LDH/g-C_3N_4 composite is shown in Fig. 10A. Mg-Al-LDH with a positive surface charge was assembled with oppositely charged g-C_3N_4 by electrostatic interaction. In the TEM image shown in Fig. 10B, the hexagonal-shaped LDH nanosheets can be seen on the surface of g-C_3N_4. Owing to its unique layered structure, CO_2 molecules can be intercalated in the interlayer space of LDH in the form of CO_3^{2-} anions. After loading Pd as the cocatalyst, CH_4 was the main product from CO_2 reduction using this photocatalyst under UV-vis light. Isotopic measurement and blank control experiment indicated that most of the evolved CH_4 was from CO_2 instead of other carbon containing species. The photocatalytic activity of the assembly system is 4 times that of the control sample without LDH. Among the LDHs intercalated with dominantly NO_3^-, dominantly CO_3^{2-} and the mixture of the two, LDH-CO_3^{2-} shows superior performance (Fig. 10C), suggesting that the intercalated CO_3^{2-} anions from dissolved CO_2 in water can act as a carbon source and are easily

reduced since LDH is in close contact with both g-C_3N_4 and Pd. As shown in Fig. 10D, LDHs with different metal compositions were compared and Mg-Al-LDH exhibited the best performance for CO_2 reduction which is correlated with the highest CO_2 adsorption capacity of Mg-Al-LDH among all LDHs. The highest QE of 0.093% was obtained at 440 nm over the optimized Pd/LDH/g-C_3N_4 assembly. The QE is still low but this example shows the concept of coupling g-C_3N_4 with a CO_2 capturing material is promising in CO_2 reduction.

In summary, the study of g-C_3N_4 based photocatalysts for CO_2 reduction is still at its early stage, but has received increasing interests in recent years. Different g-C_3N_4 based photocatalysts were synthesized including organic-inorganic hybrids, metal deposited g-C_3N_4, nanocomposites of g-C_3N_4 with oxides or carbon materials, and composites of g-C_3N_4 with CO_2 adsorbing materials. The photocatalytic activity of g-C_3N_4 based photocatalysts depends on many factors and continuous efforts are needed for the development of more efficient and stable photocatalysts for CO_2 reduction. It is also worth noting that the reported experiment setups, reaction conditions and product analysis methods vary from one paper to another. This makes it difficult to directly compare the reported activity data from different research groups. While it is challenging to adopt the same experimental setup by different groups, it is important to use reliable methods to accurately quantify various products of CO_2 reduction. Several review articles including ours published in the past few years on this topic can provide useful practical guidelines to researchers in this field.[112-114]

6. Conclusion and Outlook

This mini review summarizes the latest research efforts on the development of g-C_3N_4 based photocatalyst systems with the emphasis on the development of non-noble metal cocatalysts for g-C_3N_4, exfoliation of g-C_3N_4 to nanosheets with enhanced photoactivity, and application of g-C_3N_4 based photocatalysts for water oxidation, overall water splitting and CO_2 reduction. The study of non-noble metal cocatalyst loaded g-C_3N_4 has already achieved some breakthroughs. The activities of a few photocatalysts like MoS_2/g-C_3N_4 and $Ni(OH)_2$/g-C_3N_4 were reported to approach or surpass those of Pt/g-C_3N_4. Further improvement of efficiency and stability is still in need. Exfoliation is a promising method to improve the photocatalytic activity of g-C_3N_4. Facile and simple liquid exfoliation can be conducted in water, certain organic solvents or acid solutions. Single layered or few layered g-C_3N_4 nanosheets can be obtained after exfoliation. The larger surface area, improved charge transfer ability and enhanced charge separation contribute to the superior photocatalytic activities of g-C_3N_4 nanosheets. The performance can be further improved by preparing porous g-C_3N_4 nanosheets. However, the current exfoliation method suffers from long time sonication and low yield. It is necessary to develop more efficient exfoliation methods. Water oxidation can be achieved by g-C_3N_4 based photocatalysts such as cobalt oxides loaded g-C_3N_4, although there are only limited research works on water oxidation over g-C_3N_4. The performance and stability of current g-C_3N_4 water oxidation photocatalysts are quite poor. Meanwhile, the study of overall water splitting by g-C_3N_4 based photocatalysts is in its early stage although some systems including single particulate system and Z scheme have been shown capable of evolving stoichiometric H_2 and O_2 from water. Further development of efficient g-C_3N_4 based photocatalysts for water oxidation is thus needed for its application in overall water splitting. There have been increasing research interests on CO_2 photoreduction using g-C_3N_4 owing to its suitable electronic band structure. Drawbacks including moderate optical adsorption property, low charge carrier mobility, inert surface, low surface area and rich grain boundary defects need to be overcome to improve its photocatalytic activity. Some innovative ways and more systematic work are probably required to develop g-C_3N_4 to efficient and stable photocatalysts, which is a challenging task.

Acknowledgement

This work was supported by Nanyang Technological University. S.M. Yin acknowledges the research scholarship from Nanyang Technological University.

Notes and references

1 D. Kim, K. K. Sakimoto, D. Hong and P. Yang, *Angew. Chem. Int. Ed.*, 2015, **54**, 3259.
2 T. Hisatomi, J. Kubota and K. Domen, *Chem. Soc. Rev.*, 2014, **43**, 7520.
3 S. N. Habisreutinger, L. Schmidt-Mende and J. K. Stolarczyk, *Angew. Chem. Int. Ed.*, 2013, **52**, 7372.
4 A. Fujishima and K. Honda, *Nature*, 1972, **238**, 37.
5 A. Kudo and Y. Miseki, *Chem. Soc. Rev.*, 2009, **38**, 253.
6 F. E. Osterloh, *Chem. Soc. Rev.*, 2013, **42**, 2294.
7 K. Maeda and K. Domen, *MRS Bull.*, 2011, **36**, 25.
8 A. J. Morris, G. J. Meyer and E. Fujita, *Acc. Chem. Res.*, 2009, **42**, 1983.
9 S. Cao, J. Low, J. Yu and M. Jaroniec, *Adv. Mater.*, 2015, **27**, 2150.
10 Y. Wang, X. C. Wang and M. Antonietti, *Angew. Chemie. Int. Ed.*, 2012, **51**, 68.
11 X. C. Wang, K. Maeda, A. Thomas, K. Takanabe, G. Xin, J. M. Carlsson, K. Domen and M. Antonietti, *Nat. Mater.*, 2009, **8**, 76.
12 Y. Moriya, T. Takata and K. Domen, *Coord. Chem. Rev.*, 2013, **257**, 1957.
13 X. Ma, Y. Lv, J. Xu, Y. Liu, R. Zhang and Y. Zhu, *J. Phys. Chem. C*, 2012, **116**, 23485.
14 Y. Zhang, T. Mori, J. Ye and M. Antonietti, *J. Am. Chem. Soc.*, 2010, **132**, 6294.
15 G. Liu, P. Niu, C. Sun, S. C. Smith, Z. Chen, G. Q. M. Lu and H. Cheng, *J. Am. Chem. Soc.*, 2010, **132**, 11642.
16 G. Dong, K. Zhao and L. Zhang, *Chem. Commun.*, 2012, **48**, 6178.
17 Y. Zhang, T. Mori and J. Ye, *Sci. Adv. Mater.*,2012, **4**, 282.
18 Z. Lin and X. Wang, *Angew. Chem. Int. Ed.*, 2013, **52**, 1735.
19 M. Zhang and X. Wang, *Energy Environ. Sci.*, 2014, **7**, 1902.

20 X. Wang, X. Chen, A. Thomas, X. Fu and M. Antonietti, *Adv. Mater.*, 2009, **21**, 1609.
21 G. Zhang, M. Zhang, X. Ye, X. Qiu, S. Lin and X. Wang, *Adv. Mater.*, 2014, **26**, 805.
22 J. Hong, X. Xia, Y. Wang and R. Xu, *J. Mater. Chem.*, 2012, **22**, 15006.
23 P. Martin-Ramos, J. Martin-Gil, R. Dante, F. Vaquero, R. Navarro and J. Fierro, *Int. J. Hydrogen Energy*, 2015, **40**, 7273.
24 Y. Zhang, T. Mori, L. Niu and J. Ye, *Energy Environ. Sci.*, 2011, **4**, 4517.
25 Q. Xiang, J. Yu and M. Jaroniec, *J. Phys. Chem. C*, 2011, **115**, 7355.
26 A. Du, S. Sanvito, Z. Li, D. Wang, Y. Jiao, T. Liao, Q. Sun, Y. H. Ng, Z. Zhu, R. Amal and S. C. Smith, *J. Am. Chem. Soc.*, 2012, **134**, 4393.
27 X. Wang, J. Chen, X. Guan and L. Guo, *Int. J. Hydrogen Energy*, 2015, **40**, 7546.
28 Z. Zhao, Y. Sun and F. Dong, *Nanoscale*, 2015, **7**, 15.
29 Y. Wang, J. Hong, W. Zhang and R. Xu, *Catal. Sci. Technol.*, 2013, **3**, 1703.
30 L. Ge, F. Zuo, J. Liu, Q. Ma, C. Wang, D. Sun, L. Bartels and P. Feng, *J. Phys. Chem. C*, 2012, **116**, 13708.
31 X. Wang, K. Maeda, X. Chen, K. Takanabe, K. Domen, Y. Hou, X. Fu and M. Antonietti, *J. Am. Chem. Soc.*, 2009, **131**, 1680.
32 J. Zhang, M. Zhang, C. Yang and X. Wang, *Adv. Mater.*, 2014, **26**, 4121.
33 Y. Cui, Z. Ding, X. Fu and X. Wang, *Angew. Chem. Int. Ed.*, 2012, **51**, 11814.
34 X. Li, X. Wang and M. Antonietti, *Chem. Sci.*, 2012, **3**, 2170.
35 X. Bai, L. Wang, R. Zong and Y. Zhu, *J. Phys. Chem. C*, 2013, **117**, 9952.
36 D. Zheng, C. Pang, Y. Liu and X. Wang, *Chem. Commun.*, 2015, **51**, 9706.
37 J. H. Sun, J. S. Zhang, M. W. Zhang, M. Antonietti, X. Z. Fu and X. C. Wang, *Nat. Commun.*, 2012, **3**, 1139.
38 J. Zhang, F. Guo and X. Wang, *Adv. Funct. Mater.*, 2013, **23**, 3008.
39 S. Cao and J. Yu, *J. Phys. Chem. Lett.*, 2014, 2101.
40 J. Yang, D. Wang, H. Han and C. Li, *Acc. Chem. Res.*, 2013, **46**, 1900.
41 J. Ran, J. Zhang, J. Yu, M. Jaroniec and S. Z. Qiao, *Chem. Soc. Rev.*, 2014, **43**, 7787.
42 J. Dong, M. Wang, X. Li, L. Chen, Y. He and L. Sun, *ChemSusChem*, 2012, **5**, 2133.
43 D. Wang, Y. Zhang and W. Chen, *Chem. Commun.*, 2014, **50**, 1754.
44 J. Huang, K. L. Mulfort, P. Du and L. X. Chen, *J. Am. Chem. Soc.*, 2012, **134**, 16472.
45 S. Cao, X. Liu, Y. Yuan, Z. Zhang, J. Fang, S. C. J. Loo, J. Barber, T. C. Sum and C. Xue, *Phys. Chem. Chem. Phys.*, 2013, **15**, 18363.
46 S. Cao, Y. Yuan, J. Barber, S. C. J. Loo and C. Xue, *Appl. Surf. Sci.*, 2014, **319**, 344.
47 J. Hong, Y. Wang, Y. Wang, W. Zhang and R. Xu, *ChemSusChem*, 2013, **6**, 2263.
48 Z. Chen, P. Sun, B. Fan, Z. Zhang and X. Fang, *J. Phys. Chem. C*, 2014, **118**, 7801.
49 L. Yin, Y. Yuan, S. Cao, Z. Zhang and C. Xue, *RSC Adv.*, 2014, **4**, 6127.
50 Y. Zhu, Y. Xu, Y. Hou, Z. Ding and X. Wang, *Int. J. Hydrogen Energ.*, 2014, **39**, 11873.
51 H. Vrubel, D. Merki and X. Hu, *Energy Environ. Sci.*, 2012, **5**, 6136.
52 Y. Hou, A. B. Laursen, J. Zhang, G. Zhang, Y. Zhu, X. Wang, S. Dahl and I. Chorkendorff, *Angew. Chem. Int. Ed.*, 2013, **52**, 3621.
53 Y. Hou, Y. Zhu, Y. Xu and X. Wang, *Appl. Catal. B*, 2014, **156-157**, 122.
54 J. Yu, S. Wang, B. Cheng, Z. Lin and F. Huang, *Catal. Sci. Technol.*, 2013, **3**, 1782.
55 X. Zhou, Z. Luo, P. Tao, B. Jin, Z. Wu and Y. Huang, *Mater. Chem. Phys.*, 2014, **143**, 1462.
56 G. Zhang, G. Li and X. Wang, *ChemCatChem*, 2015. doi: 10.1002/cctc.201500069.
57 P. Niu, L. Zhang, G. Liu and H. Cheng, *Adv. Funct. Mater.*, 2012, **22**, 4763.
58 H. Xu, J. Yan, X. She, L. Xu, J. Xia, Y. Xu, Y. Song, L. Huang and H. Li, *Nanoscale*, 2014, **6**, 1406.
59 X. Zhang, X. Xie, H. Wang, J. Zhang, B. Pan and Y. Xie, *J. Am. Chem. Soc.*, 2012, **135**, 18.
60 J. Tian, Q. Liu, A. M. Asiri, A. O. Al-Youbi and X. Sun, *Anal. Chem.*, 2013, **85**, 5595.
61 N. Cheng, J. Tian, Q. Liu, C. Ge, A. H. Qusti, A. M. Asiri, A. O. Al-Youbi and X. Sun, *ACS Appl. Mater. Interfaces*, 2013, **5**, 6815.
62 H. Zhang, L. Guo, L. Zhao, B. Wan and Y. Yang, *J. Phys. Chem. Lett.*, 2015, 958.
63 S. Yang, Y. Gong, J. Zhang, L. Zhan, L. Ma, Z. Fang, R. Vajtai, X. Wang and P. M. Ajayan, *Adv. Mater.*, 2013, **25**, 2452.
64 X. She, H. Xu, Y. Xu, J. Yan, J. Xia, L. Xu, Y. Song, Y. Jiang, Q. Zhang and H. Li, *J. Mater. Chem. A*, 2014, **2**, 2563.
65 Q. Lin, L. Li, S. Liang, M. Liu, J. Bi and L. Wu, *Appl. Catal. B*, 2015, **163**, 135.
66 H. Zhao, H. Yu, X. Quan, S. Chen, Y. Zhang, H. Zhao and H. Wang, *Appl. Catal. B*, 2014, **152-153**, 46.
67 J. Hong, S. Yin, Y. Pan, J. Han, T. Zhou and R. Xu, *Nanoscale*, 2014, **6**, 14984.
68 K. Chang, M. Li, T. Wang, S. Ouyang, P. Li, L. Liu and J. Ye, *Adv. Energy Mater.*, 2015, **5**. doi: 10.1002/aenm.201402279.
69 J. Xu, L. Zhang, R. Shi and Y. Zhu, *J. Mater. Chem. A*, 2013, **1**, 14766.
70 F. Cheng, H. Wang and X. Dong, *Chem. Commun.*, 2015, **51**, 7176.
71 J. Duan, S. Chen, M. Jaroniec and S. Z. Qiao, *ACS Nano*, 2015, **9**, 931.
72 Y. Hou, F. Zuo, A. P. Dagg, J. Liu and P. Feng, *Adv. Mater.*, 2014, **26**, 5043.
73 Y. Zhao, F. Zhao, X. Wang, C. Xu, Z. Zhang, G. Shi and L. Qu, *Angew. Chem. Int. Ed.*, 2014, **53**, 13934.
74 T. Y. Ma, S. Dai, M. Jaroniec and S. Z. Qiao, *Angew. Chem. Int. Ed.*, 2014, **53**, 7281.
75 F. Zhang, A. Yamakata, K. Maeda, Y. Moriya, T. Takata, J. Kubota, K. Teshima, S. Oishi and K. Domen, *J. Am. Chem. Soc.*, 2012, **134**, 8348.
76 K. Maeda, X. Wang, Y. Nishihara, D. Lu, M. Antonietti and K. Domen, *J. Phys. Chem. C*, 2009, **113**, 4940.

77 A. B. Jorge, D. J. Martin, M. T. S. Dhanoa, A. S. Rahman, N. Makwana, J. Tang, A. Sella, F. Corà, S. Firth, J. A. Darr and P. F. McMillan, *J. Phys. Chem. C*, 2013, **117**, 7178.
78 M. Walter, E. Warren, J. McKone, S. Boettcher, Q. Mi, E. Santori and N. Lewis, *Chem. Rev.*, 2010, **110**, 6446.
79 J. Zhang, J. Sun, K. Maeda, K. Domen, P. Liu, M. Antonietti, X. Fu and X. Wang, *Energy Environ. Sci.*, 2011, **4**, 675.
80 J. Zhang, M. Grzelczak, Y. Hou, K. Maeda, K. Domen, X. Fu, M. Antonietti and X. Wang, *Chem. Sci.*, 2012, **3**, 443.
82 G. Zhang, S. Zang and X. Wang, *ACS Catal.*, 2015, 941.
83 R. Lee, P. D. Tran, S. S. Pramana, S. Y. Chiam, Y. Ren, S. Meng, L. H. Wong and J. Barber, *Catal. Sci. Technol.*, 2013, **3**, 1694.
83 A. Kudo, *MRS Bull.*, 2011, **36**, 32.
84 D. J. Martin, P. J. T. Reardon, S. J. A. Moniz and J. Tang, *J. Am. Chem. Soc.*, 2014, **136**, 12568.
85 G. Zhang, X. Huang, F. Fina, G. Zhang, J. Irvine, *Catal. Sci. Technol.*, 2015, **5**, 3416.
86 J. Liu, Y. Liu, N. Liu, Y. Han, X. Zhang, H. Huang, Y. Lifshitz, S. Lee, J. Zhong and Z. Kang, *Science*, 2015, **347**, 970.
87 L. Liao, Q. Zhang, Z. Su, Z. Zhao, Y. Wang, Y. Li, X. Lu, D. Wei, G. Feng, Q. Yu, X. Cai, J. Zhao, Z. Ren, H. Fang, F. Robles-Hernandez, S. Baldelli and J. Bao, *Nat. Nanotechnol.*, 2013, **9**, 69.
88 Q. Xiang, B. Cheng and J. Yu, *Angew. Chem. Int. Ed.*, 2015. doi: 10.1002/anie.201411069.
89 K. Li, X. An, L. Park, M. Khraisheh, J. Tang, *Catal. Today*, 2014, **224**, 3.
90 L. Yuan and Y. Xu, *Appl. Surf. Sci.*, 2015, **342**, 154.
91 X. Li, J. Wen, J. Low, Y. Fang and J. Yu, *Sci. China Mater.*, 2014, **57**, 70.
92 G. Dong and L. Zhang, *J. Mater. Chem.*, 2012, **22**, 1160.
93 J. Mao, T. Peng, X. Zhang, K. Li, L. Ye and L. Zan, *Catal. Sci. Technol.*, 2013, **3**, 1253.
94 K. Wang, Q. Li, B. Liu, B. Cheng, W. Ho and J. Yu, *Appl. Catal. B*, 2015, **176-177**, 44.
95 K. Maeda, K. Sekizawa and O. Ishitani, *Chem. Commun.*, 2013, **49**, 10127.
96 K. Sekizawa, K. Maeda, K. Domen, K. Koike and O. Ishitani, *J. Am. Chem. Soc.*, 2013, **135**, 4596.
97 Y. Tamaki, T. Morimoto, K. Koike and O. Ishitani, *Proc. Natl. Acad. Sci.*, 2012, **109**, 15673.
98 R. Kuriki, K. Sekizawa, O. Ishitani and K. Maeda, *Angew. Chem. Int. Ed.*, 2015, **54**, 2406.
99 K. Maeda, R. Kuriki, M. Zhang, X. Wang and O. Ishitani, *J. Mater. Chem. A*, 2014, **2**, 15146.
100 J. Lin, Z. Pan and X. Wang, *ACS Sustainable Chem. Eng.*, 2014, **2**, 353.
101 J. Yu, K. Wang, W. Xiao and B. Cheng, *Phys. Chem. Chem. Phys.*, 2014, **16**, 11492.
102 W. Ong, L. Tan, S. Chai and S. Yong, *Dalton Trans.*, 2015, **44**, 1249.
103 H. Shi, G. Chen, C. Zhang and Z. Zou, *ACS Catal.*, 2014, **4**, 3637.
104 S. Cao, X. Liu, Y. Yuan, Z. Zhang, Y. Liao, J. Fang, S. C. J. Loo, T. C. Sum and C. Xue, *Appl. Catal. B*, 2014, **147**, 940.
105 S. Zhou, Y. Liu, J. Li, Y. Wang, G. Jiang, Z. Zhao, D. Wang, A. Duan, J. Liu and Y. Wei, *Appl. Catal. B*, 2014, **158-159**, 20.
106 Z. Sun, Z. Yang, H. Liu, H. Wang and Z. Wu, *Appl. Surf. Sci.*, 2014, **315**, 360.
107 M. Li, L. Zhang, X. Fan, Y. Zhou, M. Wu and J. Shi, *J. Mater. Chem. A*, 2015, **3**, 5189.
108 Y. He, Y. Wang, L. Zhang, B. Teng and M. Fan, *Appl. Catal. B,* 2015, **168-169**, 1.
109 W. Ong, L. Tan, S. Chai and S. Yong, *Chem. Commun.*, 2015, **51**, 858.
110 S. Wang, J. Lin and X. Wang, *Phys. Chem. Chem. Phys.*, 2014, **16**, 14656.
111 J. Hong, W. Zhang, Y. Wang, T. Zhou and R. Xu, *ChemCatChem*, 2014, **6**, 2315.
112 J. Hong, W. Zhang, J. Ren and R. Xu, *Anal. Methods*, 2012, 1086.
113 A. Corma and H. Garcia, *J Catal.*, 2013, **308**, 168.
114 J. A. Herron, J. Kim, A. A. Upadhye, G. W. Huber and C. T. Maravelias, *Energy Environ. Sci.*, 2015, **8**, 126.